



Cite this: *New J. Chem.*, 2025, 49, 13189

Furan- π -EWG skeleton for narrowband NIR-emissive fluorescent dyes†

Xiaolong Lu,^{ae} Ying Zou,^e Chunlai Yang,^e Huan Ma,^e Enmin Li^{id}*^{bcd} and Hefeng Zhang^{id}*^{ef}

A novel D- π -A type skeleton of vinyl-bridged furan/thiophene and an electron-withdrawing group (FVW/TVW) was developed, and showed narrowband-emissive near-infrared (NIR) fluorescence. In particular, dimethylamino-furan/thiophene- π -isophoryl-malononitrile (TV-IM and FV-IM) with low molecular weights of 323 and 307 exhibited large Stokes shifts of 112 nm and 74 nm and NIR-I emissions at 716 nm and 730 nm with narrowband emission with full width at half maxima of 33 nm and 37 nm, respectively. The narrowband emissions of the FVW and TVW dyes were primarily attributed to their rigid and conjugated D- π -A skeleton and heavy-atom effect of sulfur and could be further attributed to the segregated and alternated positive and negative phases of their HOMO and LUMO orbitals in ground (S_0) and excited states (S_1). Moreover, the narrowband NIR-emissive TVW dyes were successfully used to monitor viscosity and fabricate fluorescent polymeric nanofiber films.

Received 28th February 2025,
Accepted 2nd June 2025

DOI: 10.1039/d5nj00912j

rsc.li/njc

1 Introduction

Small molecular fluorescent materials are widely used in cell biology research,^{1,2} environmental analysis,^{3,4} organic light-emitting diodes (OLEDs),^{5,6} cellular imaging,^{7,8} anti-counterfeiting,^{9,10} and various medical applications,^{1,5–8,11–13} owing to their good biocompatibility, low toxicity, and feasibility structural modification.^{5–8}

Compared with dyes that emit in the visible region (400–700 nm), NIR dyes (NIR-I: 700–1000 nm, NIR-II: 1000–1700 nm) have been given much focus in the past decade, especially in bioscience, owing to their unique advantages of increased tissue penetration depth, lower auto-fluorescence, lesser tissue

damage, and higher signal-to-noise ratio.^{11,14} NIR-II fluorescent molecules have been rapidly developed since CH-1055 dye was first reported by Dai and co-workers in 2016;¹⁵ although these dyes showed better penetration capacities than NIR-I dyes, NIR-II dyes could not be detected by the widely used silicon-based detector (with a response wavelength of 350–950 nm), and thus, specific detectors, such as indium–gallium–arsenic (In–Ga–As), were required. Thus, good compatibility of NIR-I dyes with silicon-based detectors makes them comparatively better for practical applications.

Currently, NIR-I fluorescent dyes mainly include rhodamine,^{16,17} Nile blue,^{18,19} squaric acid,^{20,21} porphyrin,^{22,23} cyanine,^{7,8} BODIPY,^{11,12} dicyanomethylene-4H-pyran,^{24,25} benzothiadiazoles^{26–28} and carbon dot^{29,30} derivatives, and each of these has their own advantages and disadvantages.

However, fluorescence dyes with a moderate Stokes shift and a narrow emission are desired as interference of excitation light could be eliminated, offering pure bright emission and thus a high signal-to-noise ratio in fluorescence imaging or sensing.^{31,32} Therefore, novel NIR-I fluorescent dyes exhibiting a large Stokes shift and a narrow emission are highly desired, especially in bioimaging and organic light-emitting diodes (OLEDs).

Traditional narrowband-emissive fluorescent molecules with a small full width at half maxima (FWHM) mainly include cyanine (*ca.* 30–60 nm)^{7,8} and BODIPY derivatives (*ca.* 40–80 nm);^{11,12} however, these molecules have the drawbacks of small Stokes shift, difficulty in synthesis, large molecular weight and insufficient color purity. Thermally activated delayed fluorescent dyes (TADF) with a small energy gap ($\Delta E_{ST} < 0.3$ eV) between

^a Marine Science Institute, College of Science, Shantou University, Shantou 515063, China

^b The Key Laboratory of Molecular Biology for High Cancer Incidence Coastal Chaoshan Area, Department of Biochemistry and Molecular Biology, Shantou University Medical College, Shantou 515041, Guangdong, China.
E-mail: nmli@stu.edu.cn

^c The Laboratory for Cancer Molecular Biology, Shantou Academy Medical Sciences, Shantou 515041, China

^d Chaoshan Branch of State Key Laboratory for Esophageal Cancer Prevention and Treatment, Shantou 515063, China

^e Department of Chemistry, Key Laboratory for Preparation and Application of Ordered Structural Materials of Guangdong Province, College of Chemistry and Chemical Engineering, Shantou University, Shantou 515063, China.
E-mail: hfzhang@stu.edu.cn

^f Guangdong Engineering Technology Research Center of Advanced Polymer Synthesis, College of Chemistry and Chemical Engineering, Shantou University, Shantou 515063, China

† Electronic supplementary information (ESI) available. See DOI: <https://doi.org/10.1039/d5nj00912j>

the S_1 and T_1 states and excellent fluorescence quantum efficiency, brightness, and color coordinates have received considerable attention.³³ However, owing to the significant vibrational coupling between S_0 and S_1 , along with the remarkable structure relaxations of the S_1 state, regular TADF fluorophores show a wide emission spectrum, with their FWHM as large as 70–100 nm.^{33–35} Multiple resonance (MR) effect achieved by precisely doping electron-deficient boron (B) and electron-rich nitrogen (N) atoms simultaneously in the polycyclic aromatic hydrocarbon skeleton can endow polycyclic aromatic hydrocarbons with unique narrowband TADF properties.³⁶ For example, DABAN-1 exhibited an ultra-pure blue fluorescence emission at 459 nm with an FWHM of 28 nm.³⁶ Later, various MR-TADF fluorophores with much narrower emissions were reported, and recently, an FWHM of 13 nm was achieved.^{37,38} Nevertheless, the maximum emission wavelengths of these MR-TADF materials are limited to blue and green regions in most cases,^{39–42} except for a very few MR-TADF molecules exhibiting a small FWHM in the red or near-infrared region.^{43–50} To achieve long-wavelength emission, the substitution base of B atoms could be further increased to achieve the multiple boronization of molecules (*e.g.*, as in the triple-B-containing MR-TADF ω -DABNA).⁴³ On the other hand, *para* B- π -B/N- π -N structures promise an efficient strategy for narrowing the energy gap.^{44,45} Yasuda *et al.* reported the first red MR emitter BBCz-R (λ_{em} = 615 nm) with a FWHM of 22 nm.⁴⁵ Yang *et al.* designed and synthesized MR emitters that enable the fabrication of high-performance narrowband green to red OLEDs, with the emitters exhibiting emission peaks at 520, 562 and 606 nm with narrow FWHMs of 45, 40 and 35 nm, respectively.⁴² Duan and co-workers developed a series of NIR MR emitters with narrow emission, including R-TBN (λ_{em} = 692 nm, FWHM = 38 nm),⁴⁶ R-BN (λ_{em} = 672 nm, FWHM = 38 nm)⁴⁷ and BNNO (λ_{em} = 637 nm, FWHM = 38 nm).⁴⁸ However, it is still challenging to design and synthesize NIR MR emitters. The only successes were achieved by Liu and Wang's group, which developed a series of double B-N-bridged bipyridine (BNBP)-based homopolymers with NIR emission, a high fluorescence quantum (Φ_F = *ca.* 0.7) and narrow emission, *i.e.*, PB-FO (λ_{em} = 705 nm, FWHM = 52 nm), PB-FPA (λ_{em} = 716 nm, FWHM = 49 nm) and PB-FPO (λ_{em} = 728 nm, FWHM = 48 nm).⁵⁰

In recent years, fluorescent nano-fibers have attracted increasing attention due to their potential application in sensing, anti-counterfeiting, wearable fluorescent displays, anti-bacterial and information encryption fields.^{51–55} Tang's group reported a kind of flexible PAN/PVP/PEG/Py-CH/SiO₂@h-BN composite fiber textile. The multifunctional composite textile could be widely applied in fluorescence anti-counterfeiting, alcohol sensing and flexible body heat management.⁵² Wu and co-workers prepared a series of highly stable and tunable fluorescent flexible hollow cellulose-based microsphere films through a crosslinking copolymerization and self-assembly strategy, which showed potential application in fields such as safety warnings, smart labels, light-emitting devices and anti-counterfeiting materials.⁵³ Qi *et al.* prepared acetylacetate cellulose fluorescent fibers with clustering-triggered emission for the first time through a laboratory-scale pilot

wet-spinning machine, and the obtained fibers demonstrated potential application in fields such as information encryption, wearable fluorescent displays and fluorescent handicrafts.⁵⁴

Developing novel narrowband NIR-emissive fluorophores, especially those with small molecular weights, simple skeletons, large Stokes shifts and easy synthesizability, is highly meaningful for extending their applications, such as in bioimaging. Very recently, we synthesized a series of functionalized hydrostyryl pyridium (HSW) compounds, which showed tunable emission covering a wide range from blue to near infrared.^{56,57} Interestingly, unexpected narrowband emission was accidentally observed when the phenyl group was replaced by a furan and thiophene ring, which implied a novel skeleton for narrowband-emissive emitters. In this work, we designed and synthesized a series of novel red- and NIR-emissive emitters of FVW (furan-vinyl-EWG) and TVW (thiophene-vinyl-EWG) derivatives with low molecular weights and the typical D- π -A structure of π -bridged dimethylamino-functionalized furan/thiophene (donor group) and an electron-withdrawing group of malonitrile or a pyridyl quaternary ammonium group (acceptor group). Due to the efficient intramolecular charge transfer, the resulting dyes showed narrowband red and NIR emission with a FWHM as low as 33 nm. The successful synthesis of the FVW and TVW families promises a feasible way to design narrowband-emissive dyes in a wide-wavelength region with small molecular weights and large Stokes shifts.

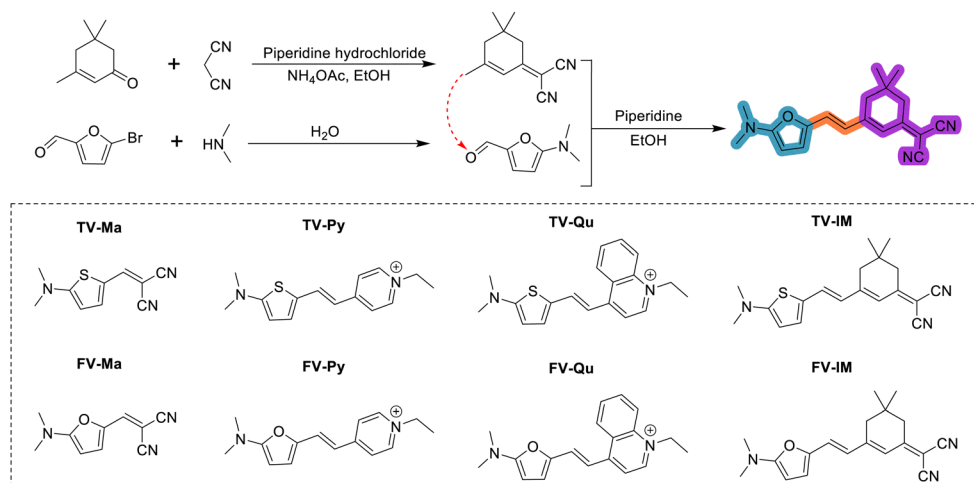
2 Results and discussion

2.1 Synthesis and characterization of fluorescent dyes of FVW families

The synthesis of FVW is shown in Scheme 1. As an example, (dimethylamino)furan-vinyl-isophoryl-malononitrile (FV-IM) was synthesized by the Knoevenagel condensation of 2-(3,5,5-trimethylcyclohex-2-en-1-ylidene)malononitrile (isophoryl-malononitrile) (electron-withdrawing group, IM) pre-synthesized by a malonitrile-isophorone Knoevenagel condensation and 5-(dimethylamino) furan-2-carbaldehyde (electron-donating group, FV), pre-synthesized by the nucleophilic attack of dimethylamine to 5-bromofuran-2-carbaldehyde. By varying the furan to thiophene group ratio and extending the EWG to aromatic quaternary ammonium groups, a series of FVW and TVW derivatives were synthesized using the same synthesis strategy. All the intermediates and the final products were characterized and confirmed by ¹H and ¹³C nuclear magnetic resonance spectroscopy (NMR) (see the Experimental section in the ESI†).

2.2 Narrowband emission characteristics of fluorescent molecules

All the resultant FVW and TVW dyes showed significant fluorescence in dimethylsulfoxide (DMSO) solution (Table 1). Furan-vinyl-Malonitrile (FV-Ma) showed a yellow color in daylight due to its strong absorption in the blue range (λ_{abs} = 468 nm) and coincidentally, it exhibited a similar yellow emission (λ_{em} = 554 nm) due to its moderate Stokes shift of 86 nm. Extending



Scheme 1 Synthetic routes of fluorescent dyes of the FVW family.

Table 1 Photoluminescent characteristics of fluorescent molecules in DMSO

Sample	MW ^a	$\lambda_{\text{abs}}^b/\text{nm}$	$\lambda_{\text{em}}^c/\text{nm}$	$\epsilon \times 10^5/\text{L mol}^{-1} \text{ cm}^{-1}$	Stokes shift ^c /nm	FWHM ^c /nm	$\Phi^d/\%$	I_{em}^e
FV-Ma	187	468	554	6.56	86	82	2.2	14 432
FV-IM	307	656	730	0.48	74	37	2.4	1150
FV-Py	323	550	631	0.72	81	43	1.3	941
FV-Qu	373	655	727	1.68	72	60	0.5	841
TV-Ma	203	466	514	0.74	48	57	1.7	1254
TV-IM	323	604	716	0.36	112	33	3.0	1088
TV-Py	339	535	627	1.11	92	36	1.2	1332
TV-Qu	389	625	739	9.68	114	64	0.6	5808

^a MW, Molecular weight. ^b Maximum absorptions measured in DMSO solution ($c = 1.0 \times 10^{-6} \text{ M}$). ^c Maximum emissions measured in DMSO solution ($c = 1.0 \times 10^{-5} \text{ M}$). ^d Absolute photoluminescence quantum yields of the dyes in DMSO solution determined using the integrating sphere method. ^e Brightness (I_{em}) = $\epsilon \times \Phi$.

the π -bridge by inserting an isophenyl moiety between vinyl group and the malonitrile group resulted in FV-IM, which showed significantly red-shifted emission in the NIR region ($\lambda_{\text{em}} = 730 \text{ nm}$), indicating that the furan ring was better for the design of long-wavelength emissive fluorescent dyes than the phenyl ring, as observed by comparing the performance with HSW derivatives in our previous work.^{57,58} Surprisingly, an unexpected narrowband emission (FWHM = 37 nm) was shown by FV-IM. Its small molecular size (MW = 307, $\lambda_{\text{em}} = 730 \text{ nm}$), moderate Stokes shift (74 nm) and narrowband emission make FV-IM attractive for practical applications. To better explore their emission behaviors and mechanisms of FVW, the EWG of FVW was further extended to pyridinium and quinolinium, resulting in the red-emissive FV-Py ($\lambda_{\text{em}} = 631 \text{ nm}$) and NIR-emissive FV-Qu ($\lambda_{\text{em}} = 727 \text{ nm}$) with FWHMs of 43 and 60 nm, respectively. The NIR emission of FV-Qu was attributed to the enlarged conjugated structure of quinolinium, which narrowed the energy gap between the excitation and ground state; however, this also led to a larger structural relaxation of the molecules⁴⁹ and caused a significant energy level splitting, resulting in a wide FWHM.

Moreover, considering the better electron delocalization capacity of the sulfur atom than oxygen atom, thiophene was used to replace the furan ring. The resultant TVW dyes also

showed significant fluorescence in the wavelength range from 514 to 739 nm (Fig. 1, Table 1 and Fig. S1, ESI†). Compared with the 5-dimethylaminofuran derivatives, the 5-dimethylaminothiophene derivatives showed a narrower FWHM, which was attributed to their suppressed structural relaxation and vibration coupling due to the heavy-atom effect of the sulfur atom.^{58,59} Thiophene-vinyl-Malonitrile (TV-Ma) exhibited a FWHM of 57 nm, which was further suppressed to 33 nm when the malonitrile group was replaced by isophenyl malonitrile. Among the EWGs, isophenyl malonitrile showed the best performance in terms of the emission red-shift and narrowband emission in both the FVW and TVW dyes. The suppression of the FWHM from FV-Ma to FV-IM and TV-Ma to TV-IM both indicated that prolonging the π vinyl group suppressed the FWHM due to the rigidity of the cyclic structure introduced by the isophenone. In addition, similar to FV-Qu, TV-Qu also showed a long-wavelength emission ($\lambda_{\text{em}} = 739 \text{ nm}$) and a wide FWHM of 64 nm.

Furthermore, to verify the effect of the substituted group on the furan and thiophene, unsubstituted FV-IM was synthesized using the same strategy, and exhibited a wide emission, indicating that the strong electron electron-donating group played an indispensable role in narrowband emission (see Fig. S3 in the ESI†).

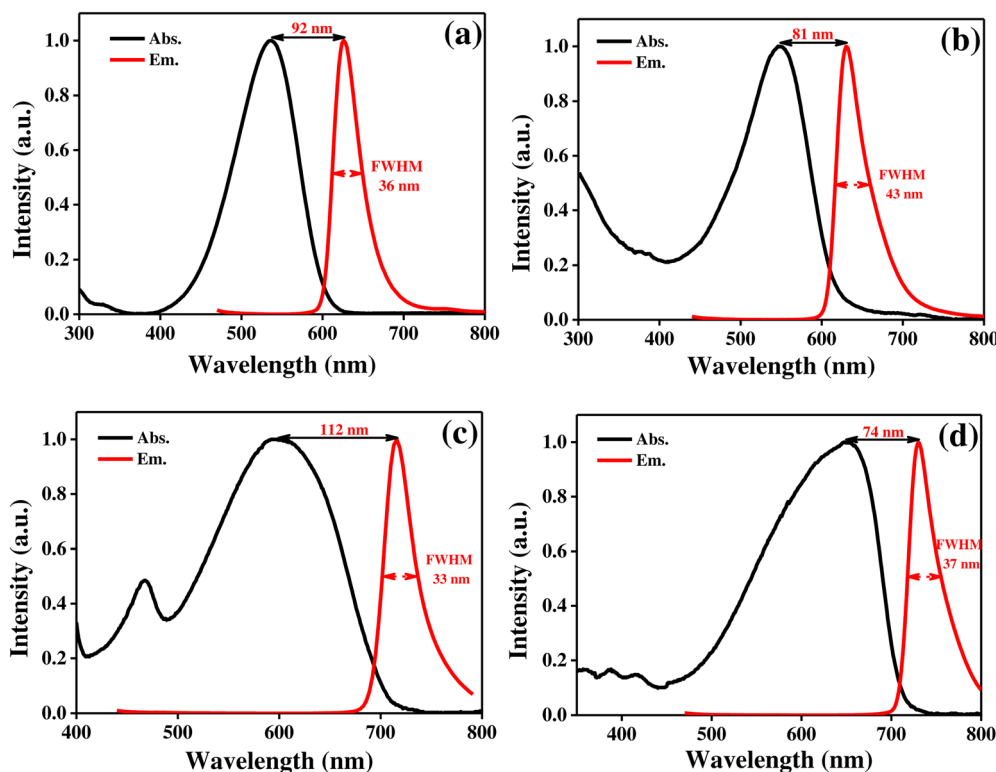


Fig. 1 Normalized absorption and luminescent spectra of fluorescent molecules, (a) TV-Py ($\lambda_{\text{ex}} = 450$ nm), (b) FV-Py ($\lambda_{\text{ex}} = 420$ nm), (c) TV-IM ($\lambda_{\text{ex}} = 420$ nm), and (d) FV-IM ($\lambda_{\text{ex}} = 450$ nm). (UV-Vis absorption spectra of the samples were recorded in DMSO solutions with concentration of $c_1 = 1.0 \times 10^{-6}$ M, fluorescent emission spectra were measured at concentration of $c_2 = 1.0 \times 10^{-5}$ M).

2.3 Solvent-dependent absorption and emission of the fluorescent molecules

To disclose the influence of the solvent over the fluorescence behaviors of the dyes, the absorption and emission spectra of FVW and TVW dyes were measured in a series of solvents with different polarities. All the fluorescent molecules showed significant solvent-dependent absorption and fluorescent behaviors (Fig. 2 and Fig. S4–S6, Tables S2–S9, ESI†). It was found that the ionic dyes FV-Py and FV-Qu showed a large absorption wavelength in low-polar solvents like dichloromethane (DCM), while the non-ionic dyes of FV-Ma and FV-IM showed a large absorption wavelength in high-polar solvents, like DMSO. For example, the ionic dye of FV-Py showed a maximum absorption at $\lambda_{\text{abs}} = 580$ nm in low-polar DCM, which was larger than the $\lambda_{\text{abs}} = 550$ nm in the high-polar DMSO. In contrast, the non-ionic dye of FV-IM showed a larger absorption wavelength of $\lambda_{\text{abs}} = 656$ nm in high-polar DMSO than that of $\lambda_{\text{abs}} = 585$ nm in low-polar DCM. The unexpected long absorption wavelength was attributed to the stronger aggregation of ionic dyes in low-polar solvents than in polar solvents, leading to a significantly enhanced π – π stacking effect and thus a decreased energy gap between the ground state and excited states, which well agreed with the effect of high concentration causing a red-shift of the absorption and fluorescence (*vide infra*).

UV absorption occurs when valence electrons are excited by light with a specific wavelength and transition from the ground

state to higher energy excited states. Compared with other molecules, FV-IM and TV-IM have rigid structures and a high similarity of structures at different excited states to that at the ground state, resulting in non-specific excited states ($S_0 \rightarrow S_n$) in the presence of an exciting light, thus causing wide absorptions, whereas the narrowed emissions were due to Kasha's rule. Density functional theory (DFT) computation results disclosed that both FV-IM and TV-IM were excited to up to five exciting states above the ground state (S_0), which was more than the three exciting states in the other TVW and FVW dyes (Fig. S7, S8 and Table S1, ESI†). The multi-exciting pathways broaden the absorption spectra of FV-IM and TV-IM because of the Franck–Condon principle.

Meanwhile, solvent dependence was also found in the fluorescent behaviors of all the dyes. Compared with the other solvents, all the FVW and TVW dyes showed the longest wavelength in DMSO with high polarity and DCM with low polarity. In particular, all the dyes showed absorption in the long wavelength, with a much higher molar extinction coefficient and higher fluorescence quantum efficiency and thus higher brightness than in the other solvents. In addition, in high-polar DMSO solution, the FVW and TVW dyes showed the narrowest emission wavelength in most cases. For example, both FV-IM and TV-IM showed NIR narrowband emission in DMSO solution (Fig. 2) with λ_{em} FWHMs of 730/37 and 716 nm/33 nm, respectively. On the other hand, as shown in Tables S5–S9 (ESI†), both FV-IM and TV-IM exhibited

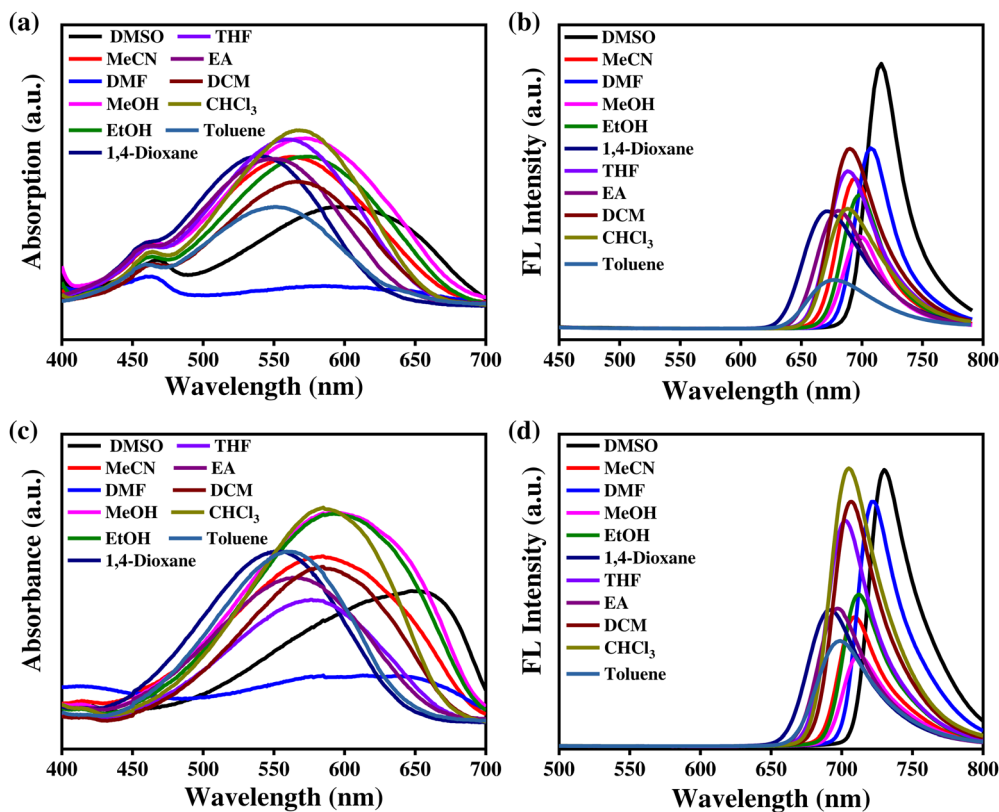


Fig. 2 UV-Vis absorption and fluorescence spectra of TV-IM and FV-IM. UV-Vis absorption spectra of TV-IM (a) and FV-IM (c) (1.0×10^{-6} M). Fluorescence spectra of TV-IM ($\lambda_{\text{ex}} = 420$ nm) (b) and FV-IM ($\lambda_{\text{ex}} = 450$ nm) (d) (1.0×10^{-5} M).

characteristic sharp narrowband NIR emissions in all solvents. Moreover, all the FVW and TVW dyes showed varied emission wavelengths within ~ 20 nm with the increase of solvent polarities for all the molecules, which suggested a short-range intramolecular charge-transfer (ICT) fluorescence mechanism.⁴⁹

2.4 Concentration-dependent emission and absorption of TV-IM

To better understand the fluorescence mechanism, the effect of concentration on the fluorescence behaviors of both the FVW and TVW dyes was explored. Taking TV-IM in DMSO and CHCl_3 as an example (Fig. 3a and b), when the concentration increased from 1 to 1000 $\mu\text{mol L}^{-1}$, the emission intensities significantly increased to a maximum at 50 $\mu\text{mol L}^{-1}$, and then gradually decreased. Moreover, with the concentration increasing, a significant red-shifting of the emission from 700 to 734 nm was observed, which was attributed to the increasingly stronger π - π stacking effect.

The concentration also affected the absorption behaviors of the dyes. Taking the solution of TV-IM in DMSO as an example, a good linear relationship ($R^2 = 0.996$) between the concentration and the absorption capacity was observed in the range 1–20 $\mu\text{mol L}^{-1}$ (Fig. 3c and d).

2.5 Theoretical calculation analysis

To better disclose their mechanism, the electronic structures of the FVW and TVW dyes as fluorescent molecules were

calculated using density functional theory (DFT) and time-dependent density functional theory (TDDFT) at the B3LYP/6-311G(d,p) level. The highest occupied molecular orbitals (HOMOs) and lowest unoccupied molecular orbitals (LUMOs) of the FVW and TVW dyes were calculated, giving their energy levels and orbital distributions (Table 2 and Table S10, ESI†). All the dyes exhibited a similar molecular orbital distribution profile, that is, the electrons were dispersed and delocalized throughout the molecular framework, which suggested the dyes had promising intramolecular charge-transfer (ICT) characteristics. It was found that the extension of the π -conjugation length effectively increased the HOMO energy level and reduced the LUMO energy level, thereby reducing the energy gap values, and meanwhile, resulted in a significant red-shifting in both the absorption and emission of TV-IM and FV-IM. The strong electron-withdrawing and conjugation structure of the EWGs significantly decreased $\Delta E_{\text{HOMO-LUMO}}$ in the order of malononitrile < pyridium < isophenyl-malononitrile < quinolinium, which agreed well with the fluorescent wavelength exhibited by both the FVW and TVW dyes (Table 1). In addition, the stronger electron-donating ability of 5-dimethylaminofuran than 5-dimethylaminothiophene suggested the FVW dyes would show a more significant ICT effect than the TVW dyes, which was proven by the lower $E_{\text{gFV-IM}}$ of 2.502 eV than $E_{\text{gTV-IM}}$ of 2.553 eV. The stronger ICT effect led to a longer emission wavelength of FVW dyes than the TVW dyes, which agreed well with the experimental results for their fluorescence behaviors.

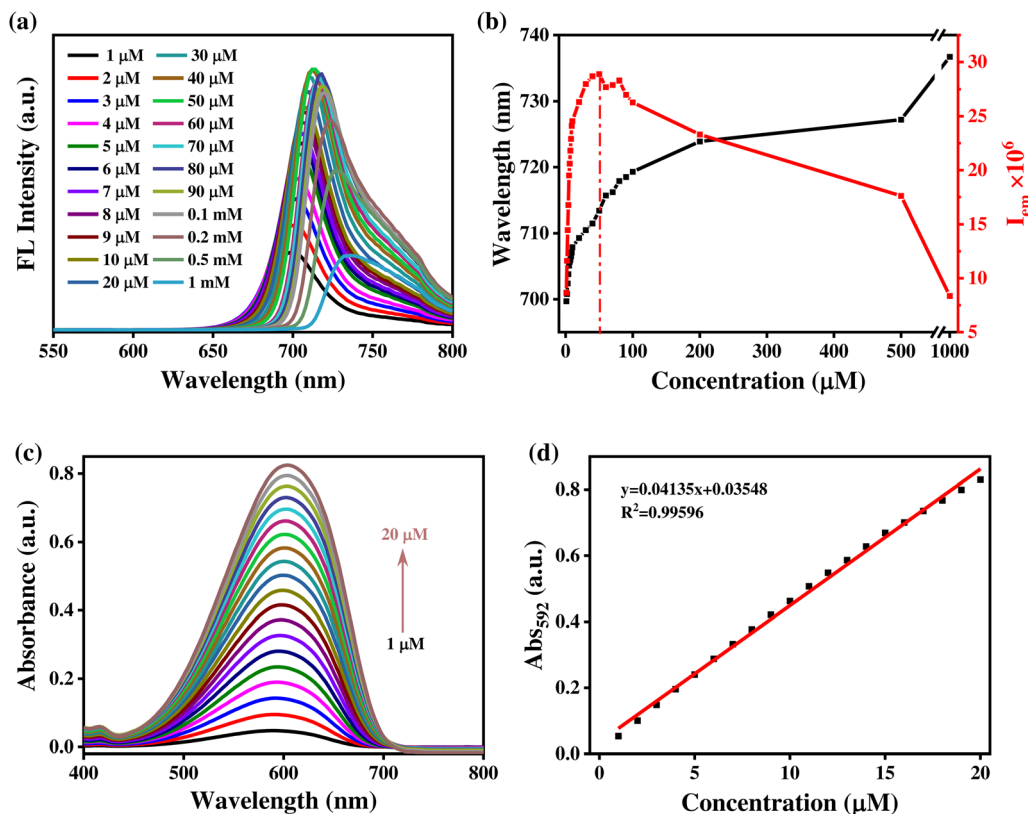


Fig. 3 Concentration-dependent fluorescent emission and absorption spectra of TV-IM, (a) and (b). Fluorescent emission spectra and relationships between emission wavelengths/intensities and concentrations in DMSO ($\lambda_{\text{ex}} = 420 \text{ nm}$). (c) and (d) Absorption spectra and relationship between the absorption capacities and concentrations in CHCl_3 .

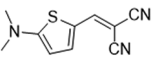
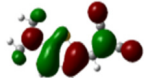
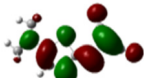
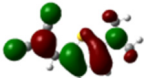
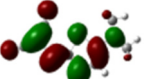
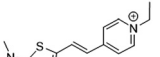
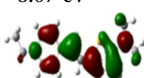
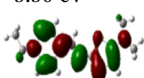

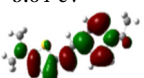
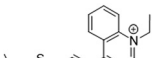

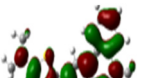
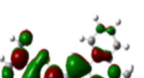
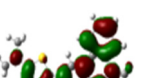
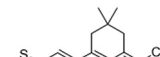
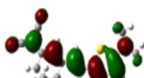

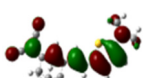
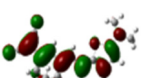
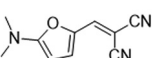
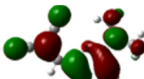
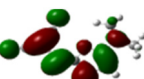
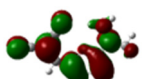
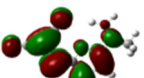
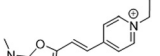
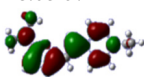
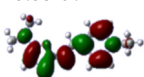
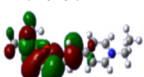
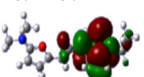
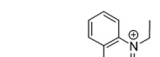
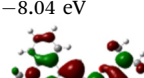

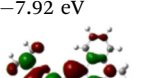
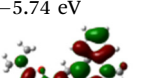
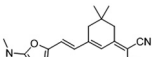
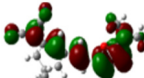
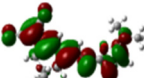
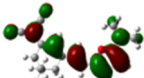
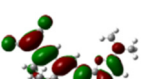
Interestingly, as mentioned above, the isophenyl-malononitrile group showed the most power to suppress the emission wavelength distribution and promised the most narrowband emission among all the groups shown in Table 1. In addition, it is worth noting that the extended π -bridge not only red-shifted the absorption and emission wavelength, but also endowed both FV-IM and TV-IM with unexpected narrowband emission characteristics. The narrowband emissions showed by FV-IM and TV-IM were attributed to the full delocalization of electrons along the skeleton, and especially, the highly uniform and ideally alternating positive and negative phases in both the HOMO and LUMO orbitals of both the ground state (S_0) and excited state (S_1). Due to the uniform and alternating orbital patterns, the $S_1 \rightarrow S_0$ transition featured a short-range recombination of electron density with prominent ICT properties, while it maintained a significant overlap of the HOMO–LUMO distribution. In addition, the alternating electron-rich and electron-deficient distributions could effectively minimize the bonding/anti-bonding properties between adjacent atoms and suppress the structural relaxation and vibrational coupling of both molecules, which suggested the FV-IM and TV-IM dyes would have a small structural displacement and thus narrowband emission spectrum, as was shown with FWHMs of 37 and 33 nm, respectively.^{38,46,60}

However, in the case of the quinolinium-containing dyes, e.g., FV-Qu and TV-Qu, the increased structural rigidity due to the quinolinium group led to a red-shifting of the absorption and emission wavelengths, while the electrons at the HOMO and LUMO levels were mainly distributed in the electron-donating group and electron-receiving group (Table 2), respectively, which resulted in no overlap of the electron distribution at the HOMO–LUMO level. The electron distribution in the electron-rich and electron-deficient patterns of the S_1 and S_0 states was different. These features caused large molecular structural relaxation and vibration coupling, which led to wide fluorescence emission spectra for FV-Qu (FWHM = 60 nm) and TV-Qu (FWHM = 64 nm).

2.6 Response of TV-IM to viscosity

During the measurement of the fluorescence behaviors, unexpected viscosity-dependent emission was observed. As an example, the viscosity-dependent emission of TV-IM in a glycerol–water mixed solvent with different viscosities (Table S11, ESI†) was recorded, as shown in Fig. 4a and b. The fluorescence intensity of TV-IM gradually increased up to 45.25-fold with the increase in viscosity tuned by increasing the glycerol ratio. The high-viscosity-enhanced emission was attributed to the restricted rotation and vibration of the skeleton in highly viscous solutions. In addition, a good linear relationship ($R^2 = 0.9775$) was observed between the emission intensity of TV-IM ($\log I_{707}$)

Table 2 HOMO/LUMO levels and molecular orbitals of FVW and TVW calculated using DFT and TD-DFT methods

Structure	S_0 (Ground state)			S_1 (Excited state)		
	HOMO	ΔE	LUMO	HOMO	ΔE	LUMO
	-5.91 eV 	3.32 eV →	-2.59 eV 	-5.87 eV 	3.12 eV →	-2.75 eV 
	-8.07 eV 	2.57 eV →	-5.50 eV 	-7.99 eV 	2.35 eV →	-5.64 eV 
	-8.05 eV 	2.44 eV →	-5.61 eV 	-7.92 eV 	2.19 eV →	-5.73 eV 
	-5.38 eV 	2.55 eV →	-2.83 eV 	-5.40 eV 	2.47 eV →	-2.93 eV 
	-5.87 eV 	3.27 eV →	-2.60 eV 	-5.85 eV 	3.06 eV →	-2.79 eV 
	-8.08 eV 	2.55 eV →	-5.53 eV 	-7.16 eV 	0.94 eV →	-6.22 eV 
	-8.04 eV 	2.42 eV →	-5.62 eV 	-7.92 eV 	2.18 eV →	-5.74 eV 
	-5.31 eV 	2.51 eV →	-2.80 eV 	-5.34 eV 	2.44 eV →	-2.90 eV 

and the viscosity ($\log \eta$), which was revealed by fitting the Förster and Hoffmann equation. To fully understand the fluorescence behaviors of TV-IM, we mixed TV-IM with different types of cations as references to check its response to the cations, which would be helpful for developing further applications. As shown in Fig. 4c and d, all the cations had negligible effects on the fluorescence of TV-IM. In contrast, glycerol could significantly enhance the fluorescence emission of TV-IM in both aqueous solution and glycerol-water solution (Fig. S9c and d, ESI†). In addition, TV-IM exhibited viscosity dependence in different polymer solutions, such as solutions of PMMA-DCM (PMMA: poly(methyl methacrylate), DCM: dichloromethane), PVA-water (PVA: poly(vinyl alcohol)), PEG-water (PEG: poly(ethylene glycol)) and PVP-water (PVP: poly(vinyl pyridine)) (Fig. S10, ESI†). The significant viscosity-dependent emission would allow TV-IM to serve as a pure color NIR fluorescent molecular probe for detecting viscosity with high selectivity and the ability to resist interference from ions^{61,62} (Fig. 4c and d).

2.7 Photoluminescent characteristics of fluorescent fibrous membranes

In addition to the viscosity probe, TV-IM and FV-IM were used as functional additives to prepare fluorescent polyvinylidene difluoride (PVDF) films. After co-dissolving with the dyes in *N,N*-dimethylacetamide (DMAc), the fluorescent fiber membranes were readily prepared using the electrospinning technique (Fig. 5). Compared with a PVDF fiber film prepared using the same method for the control and that displayed a white color in daylight and purple color under ultraviolet light, the TV-IM- and FV-IM-containing PVDF fiber membranes exhibited a blue and slight blue color in daylight, and under UV light ($\lambda_{\text{ex}} = 365 \text{ nm}$) showed fluorescent colors of bright pink and slight pink, respectively. Under daylight conditions, uniform one-dimensional fibers with diameters of $\sim 0.75 \mu\text{m}$ in the TV-IM- and FV-IM-doped PVDF fiber membranes could be clearly observed by optical microscopy, and had significantly smaller diameters than the PVDF fibers. This was mainly due to the

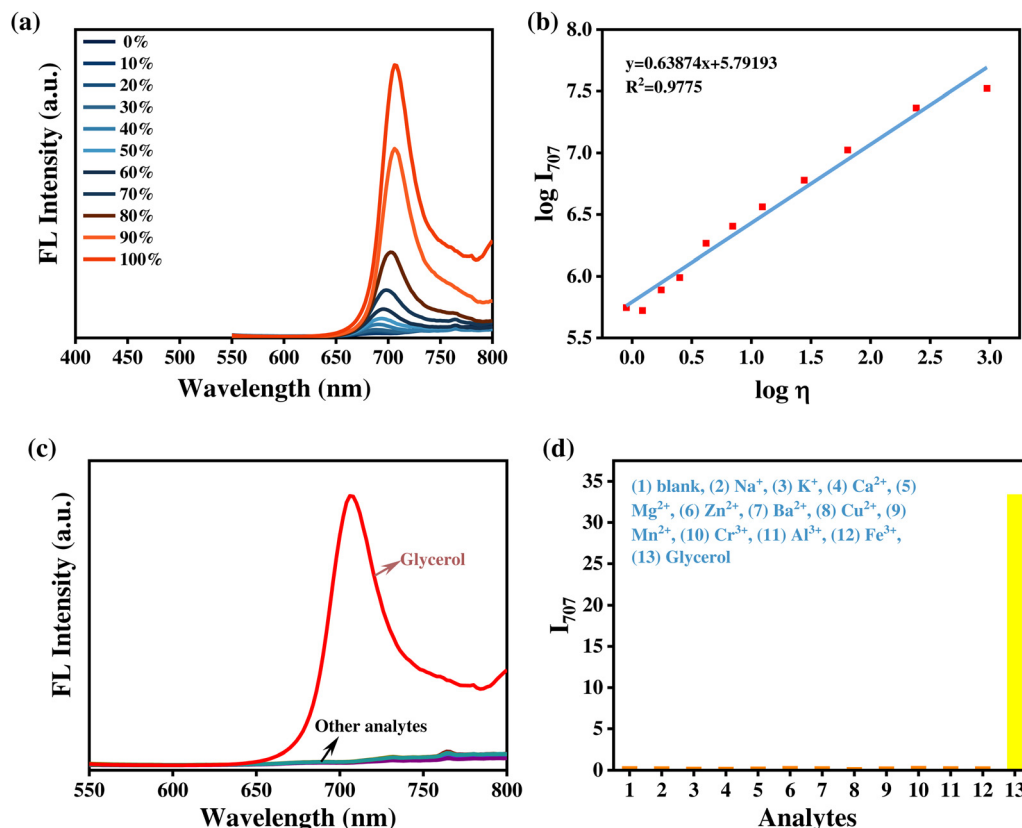


Fig. 4 (a) Fluorescence spectra of TV-IM (50 μM) with the variations in solution viscosity (glycerol fractions ($V_{\text{Gly}}\%$) was increased by 10% from bottom to top) at 23 °C. Intensity at 707 nm vs. viscosity (η) changes. (b) Linear correlation of $\log I_{707}$ and $\log \eta$. (c) Fluorescence spectra of TV-IM (50 μM) in glycerol and various ionic aqueous solutions (10 μM). (d) Corresponding fluorescence intensity of TV-IM at 707 nm for glycerol and various ions ($\lambda_{\text{ex}} = 420$ nm).

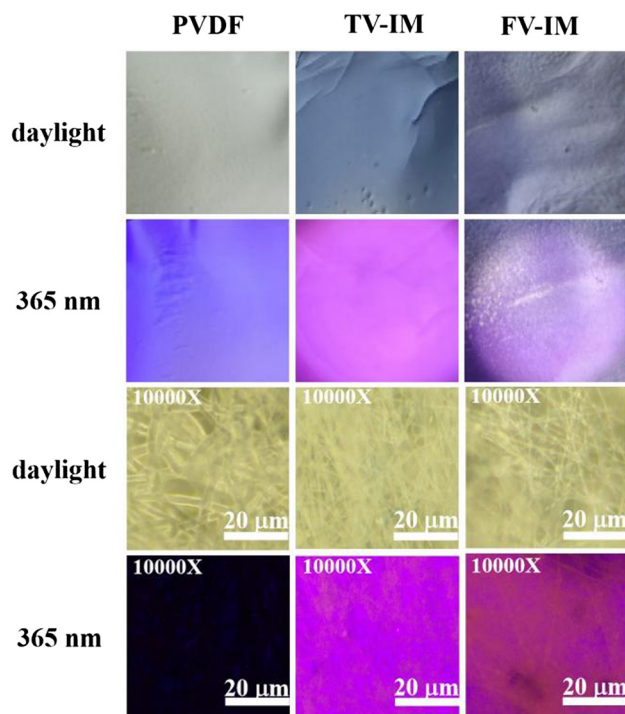


Fig. 5 Optical images of the fluorescent PVDF membranes fabricated through electrospinning using TV-IM and FV-IM as macro-additives.

conjugated structure of TV-IM and FV-IM with good conductivity, which enhanced the fiber-fragments during the electrospinning process. Under UV light ($\lambda_{\text{ex}} = 365$ nm), in contrast to the invisible PVDF pure fibers, the PVDF fluorescent fiber film doped with TV-IM and FV-IM showed bright fluorescent fibers.

3 Conclusion

In summary, we developed a novel skeleton for narrowband fluorescent emission. A series of small molecular weight fluorescent molecules were synthesized and showed narrowband emission covering the range from green to the NIR-I region. In particular, TV-IM ($\lambda_{\text{em}} = 716$ nm, FWHM = 33 nm, MW = 323, $\lambda_{\text{em}}/\text{MW} = 2.22$) and FV-IM ($\lambda_{\text{em}} = 730$ nm, FWHM = 37 nm, MW = 307, $\lambda_{\text{em}}/\text{MW} = 2.38$) showed unexpected narrowband NIR emission. In addition, TV-IM showed a significant viscosity-dependent fluorescence behavior with high selectivity. The successful synthesis of the current fluorescent molecules not only provides a reliable and low-cost synthesis strategy for constructing NIR narrowband-emissive fluorescent dyes, but also would be helpful for the development of the current fluorescence theory.

Conflicts of interest

There are no conflicts to declare.

Data availability

The data supporting this article have been included as part of the ESI.†

Acknowledgements

This work was supported by the National Natural Science Foundation of China (82273108) and Guangdong provincial Scientific and Technological Innovation Program (STKJ2023073, 2024A1515012747).

References

- H. D. Li, D. Kim, Q. C. Yao, H. Y. Ge, J. Chung, J. L. Fan, J. Y. Wang, X. J. Peng and J. Y. Yoon, *Angew. Chem.*, 2021, **133**(32), 17408–17429.
- M. K. Goshisht, N. Tripathi, G. K. Patra and M. Chaskar, *Chem. Sci.*, 2023, **14**, 5842–5871.
- Y. Wang, L. Zhang, X. Y. Han, L. W. Zhang, X. Y. Wang and L. X. Chen, *Chem. Eng. J.*, 2021, **406**, 127166.
- B. R. Jie, H. D. Lin, Y. X. Zhai, J. Y. Ye, D. Y. Zhang, Y. F. Xie, X. D. Zhang and Y. Q. Yang, *Chem. Eng. J.*, 2023, **454**, 139931.
- T. Hua, N. Li, Z. Huang, Y. Zhang, L. Wang, Z. Chen, J. Miao, X. Cao, X. Wang and C. Yang, *Angew. Chem., Int. Ed.*, 2024, **63**(7), e202318433.
- S. Wu, D. Chen, X. Zhang, D. Sun and E. Zysman-Colman, *Adv. Mater.*, 2025, **37**(8), 2415289.
- Y. H. Li, M. A. Tuttle, Q. Liu and Y. Pang, *Chem. Commun.*, 2024, **60**, 2208–2211.
- X. Z. Wang, S. S. He, P. H. Cheng and K. Y. Pu, *Adv. Mater.*, 2023, **35**, 2206510.
- Z. Gao, Y. F. Han and F. Wang, *Nat. Commun.*, 2018, **9**, 3977–3985.
- Y. Yin, Q. C. Guan, Z. Chen, D. D. Deng, S. T. Liu, Y. Sun and S. H. Liu, *Sci. Adv.*, 2024, **10**, 5444–5455.
- L. Yuan, Y. B. Su, H. L. Cong, B. Yu and Y. Q. Shen, *Dyes Pigm.*, 2022, **208**, 110851.
- Y. I. Gyasi, Y. P. Pang, X. R. Li, J. X. Gu, X. J. Cheng, J. Liu, T. Xu and Y. Liu, *Eur. J. Med. Chem.*, 2020, **187**, 111982.
- X. D. Kong, L. T. Di, Y. S. Fan, Z. K. Zhou, X. J. Feng, L. Z. Gai, J. W. Tian and H. Lu, *Chem. Commun.*, 2019, **55**, 11567–11570.
- C. Chen, R. Tian, Y. Zeng, C. C. Chu and G. Liu, *Bioconjugate Chem.*, 2020, **31**(2), 276–292.
- A. L. Antaris, H. Chen, K. Cheng, Y. Sun, G. S. Hong, C. R. Qu, S. Diao, Z. X. Deng, X. M. Hu, B. Zhang, X. D. Zhang, O. K. Yaghi, Z. R. Alamparambil, X. C. Hong, Z. Cheng and H. J. Dai, *Nat. Mater.*, 2016, **15**, 235–242.
- P. Z. Wang, L. Yu, J. K. Gong, J. H. Xiong, S. Y. Zi, H. Xie, F. Zhang, Z. Q. Mao, Z. H. Liu and J. S. Kim, *Angew. Chem., Int. Ed.*, 2022, **61**(36), e202206894.
- J. Li, Y. Dong, R. W. Wei, G. Y. Jiang, C. Yao, M. Lv, Y. Y. Wu, S. H. Gardner, F. Zhang, M. Y. Lucero, J. Huang, H. Chen, G. B. Ge, J. Chan, J. Q. Chen, H. T. Sun, X. Luo, X. H. Qian and Y. J. Yang, *J. Am. Chem. Soc.*, 2022, **144**(31), 14351–14362.
- M. Dominguez, K. Meyer, F. Sancenon, J. F. Blandez, M. Serrano and R. M. Manez, *Chem. Commun.*, 2023, **59**, 2481–2484.
- Y. Y. Zhao, L. Zhang, Z. X. Chen, B. Y. Zheng, M. R. Ke, X. S. Li and J. D. Huang, *J. Am. Chem. Soc.*, 2021, **143**(34), 13980–13989.
- J. L. Hu, B. J. Zhao, R. R. Wen, X. B. Zhang, Y. X. Zhang, D. S. Kohane and Q. Liu, *Nano Lett.*, 2023, **23**(11), 5209–5216.
- Y. Q. Lei, Y. Q. Wang, S. K. Hill, Z. H. Cheng, Q. Song and S. Perrier, *Adv. Mater.*, 2024, **36**(25), 2401346.
- Z. Y. Yang, L. F. Fan, X. Fan, M. T. Hou, Z. Y. Cao, Y. B. Ding and W. H. Zhang, *Anal. Chem.*, 2020, **92**(9), 6727–6733.
- T. V. Duncan, K. Susumu, L. E. Sinks and M. J. Therien, *J. Am. Chem. Soc.*, 2006, **128**(28), 9000–9001.
- X. Li, M. Liu, Q. Y. Yi, M. Yang, X. Y. Zhang, Y. Shi, J. J. Huang, Q. Liu, J. M. Jiang, T. T. Wei, M. Wang and J. Y. Wang, *Dyes Pigm.*, 2024, **224**, 112031.
- R. R. Wu, Z. C. Yao, Z. X. Chen, X. G. Ge, L. C. Su, S. H. Wang, Y. Wu and J. B. Song, *Anal. Chem.*, 2023, **95**(30), 11219–11226.
- H. Gu, W. J. Liu, H. D. Li, W. Sun, J. J. Du, J. L. Fan and X. J. Peng, *Coord. Chem. Rev.*, 2022, **473**, 214803.
- J.-S. Ni, P. F. Zhang, T. Jiang, Y. C. Chen, H. F. Su, D. Wang, Z. Q. Yu, R. T. K. Kwok, Z. J. Zhao, J. W. Y. Lam and B. Z. Tang, *Adv. Mater.*, 2018, **30**(50), 1805220.
- A. Abdullah, A. A. Tanriverdi, A. A. Khan, S.-J. Lee, J. B. Park, Y. S. Kim, U. Yildiko, K. Min and M. Alam, *J. Mol. Struct.*, 2024, **1304**, 137694.
- B. Y. Wang, G. I. N. Waterhouse, B. Yang and S. Y. Lu, *Acc. Chem. Res.*, 2024, **57**(19), 2928–2939.
- Y. Q. Zhang and S. Y. Lu, *Chemistry*, 2024, **10**(1), 134–171.
- H. U. Kim, T. Kim, C. Kim, M. Kim and T. Park, *Adv. Funct. Mater.*, 2023, **33**(1), 2208082.
- H. Chen, L. J. Liu, K. Qian, H. L. Liu, Z. M. Wang, F. Gao, C. R. Qu, W. H. Dai, D. Z. Lin, K. X. Chen, H. Liu and Z. Cheng, *Sci. Adv.*, 2022, **8**(32), eabo3289.
- A. Endo, K. Sato, K. Yoshimura, T. Kai, A. Kawada, H. Miyazaki and C. Adachi, *Appl. Phys. Lett.*, 2011, **98**, 083302.
- H. Uoyama, K. Goushi, K. Shizu, H. Nomura and C. Adachi, *Nature*, 2012, **492**, 234–238.
- S. Kothavale, S. C. Kim, K. Cheong, S. K. Zeng, Y. F. Wang and J. Y. Lee, *Adv. Mater.*, 2023, **35**(13), 2208602.
- T. Hatakeyama, K. Shiren, K. Nakajima, S. Nomura, S. Nakatsuka, K. Kinoshita, J. P. Ni, Y. Ono and T. Ikuta, *Adv. Mater.*, 2016, **28**(14), 2777–2781.
- Y. Kondo, K. Yoshiura, S. Kitera, H. Nishi, S. Oda, H. Gotoh, Y. Sasada, M. Yanai and T. Hatakeyama, *Nat. Photonics*, 2019, **13**, 678–682.
- X. Zeng, L. Wang, H. Y. Dai, T. Y. Huang, M. X. Du, D. Wang, D. D. Zhang and L. Duan, *Adv. Mater.*, 2023, **35**(22), 2211316.
- P. Li, W. J. Li, Y. W. Zhang, P. Zhang, X. J. Wang, C. Yin and R. F. Chen, *ACS Mater. Lett.*, 2024, **6**, 1746–1768.
- M. L. Xie, M. Z. Sun, S. F. Xue and W. J. Yang, *Dyes Pigm.*, 2022, **208**, 110799.

- 41 H. J. Kim and T. Yasuda, *Adv. Opt. Mater.*, 2022, **10**(22), 2201714.
- 42 X. C. Fan, K. Wang, Y. Z. Shi, Y. C. Cheng, Y. T. Lee, J. Yu, X. K. Chen, C. Adachi and X. H. Zhang, *Nat. Photonics*, 2023, **17**, 280–285.
- 43 S. Uemura, S. Oda, M. Hayakawa, R. Kawasumi, N. Ikeda, Y. T. Lee, C. Y. Chan, Y. Tsuchiya, C. Adachi and T. Hatakeyama, *J. Am. Chem. Soc.*, 2023, **145**(3), 1505–1511.
- 44 J. S. Miao, G. H. Chen, J. W. He, Z. Q. Xiao, X. F. Song, M. C. Wang, M. L. Huang, K. Li, X. S. Cao, Y. Zou and C. L. Yang, *Adv. Funct. Mater.*, 2024, **34**(28), 2316323.
- 45 M. L. Yang, I. S. Park and T. Yasuda, *J. Am. Chem. Soc.*, 2020, **142**(46), 19468–19472.
- 46 G. Y. Meng, J. P. Zhou, X. H. Han, W. L. Zhao, Y. W. Zhang, M. Li, C. F. Chen, D. D. Zhang and L. Duan, *Adv. Mater.*, 2024, **36**(5), 2307420.
- 47 Y. W. Zhang, D. D. Zhang, T. Y. Huang, A. J. Gillett, Y. Liu, D. P. Hu, L. S. Cui, Z. Y. Bin, G. M. Li, J. B. Wei and L. Duan, *Angew. Chem., Int. Ed.*, 2021, **60**(37), 20498–20503.
- 48 T. J. Fan, M. X. Du, X. Q. Jia, L. Wang, Z. Yin, Y. L. Shu, Y. W. Zhang, J. B. Wei, D. D. Zhang and L. Duan, *Adv. Mater.*, 2023, **35**(30), 2301018.
- 49 J. W. He, Y. L. Xu, S. Luo, J. S. Miao, X. S. Cao and Y. Zou, *Chem. Eng. J.*, 2023, **471**, 144565.
- 50 Y. Y. Gao, K. Y. Zhang, L. Zhang, S. M. Wang, H. Tong, J. Liu and L. X. Wang, *Macromolecules*, 2024, **57**(3), 1021–1029.
- 51 Z. Z. Huang, Y. X. Wang, L. J. Huang, B. Y. Li, X. H. Yan, Y. Wang, M. J. Kipper and J. G. Tang, *J. Mater. Sci.*, 2022, **57**, 2892–3922.
- 52 J. H. Lin, X. Feng, J. T. Huang, Y. W. Liu, Y. S. Xiao, Y. F. Li, Y. G. Min and B. Z. Tang, *Biosens. Bioelectron.*, 2025, **267**, 116799.
- 53 Y. J. Yao, J. N. Xue, M. Wang, D. Fu, Y. Q. Shen, Y. Xue, F. Zhang, P. B. Liu, H. R. Wang and H. L. Wu, *Chem. Eng. J.*, 2024, **482**, 149116.
- 54 C. J. Qiu, F. Peng, P. P. Wu, X. J. Wang, S. N. Hu, C. L. Huang, X. X. Li, D. F. Xu, H. Li, P. C. Ma, P. Chen and H. S. Qi, *Chem. Eng. J.*, 2024, **485**, 149869.
- 55 X. Y. Wang, Z. Zhang, S. K. Yang, J. M. Du, Y. Jiang, D. G. Miao, S. Chen, Z. L. Xiang, G. W. Xiao, C. H. Xu and S. Ramakrishna, *ACS Mater. Lett.*, 2025, **7**, 928–937.
- 56 X. Liu, F. Zhao, B. Chen, Y. F. Huang, L. Y. Xu, E. M. Li, L. L. Tan and H. F. Zhang, *Chem. – Eur. J.*, 2023, **29**(34), e202300381.
- 57 Y. W. Cheng, G. Shabir, X. Li, L. P. Fang, L. Y. Xu, H. F. Zhang and E. M. Li, *Chem. Commun.*, 2020, **56**, 1070–1073.
- 58 Y. Feng, X. M. Zhuang, Y. C. Xu, J. N. Xue, C. Qu, Q. Y. Wang, Y. Liu and Y. Wang, *Chem. Eng. J.*, 2023, **478**, 147123.
- 59 M. L. Wang, Z. Y. Fu, R. Cheng, J. P. Du, T. P. Wu, Z. Y. Bin, D. Wu, Y. D. Yang and J. B. Lan, *Chem. Commun.*, 2023, **59**, 5126–5129.
- 60 C. Y. Lv, X. Q. Wang, Q. Zhang and Y. J. Zhang, *Mater. Chem. Front.*, 2023, **7**, 2809–2827.
- 61 M. L. Fu, Y. Sun, Kenry, M. Zhang, H. H. Zhou, W. Shen, Y. Hu and Q. Zhu, *Chem. Commun.*, 2021, **57**, 3508–3511.
- 62 J. Z. Zhang, S. Y. Gong, Y. J. Liu, Z. P. Zheng and G. Q. Feng, *Sens. Actuators, B*, 2024, **406**, 135432.